Resolving biomolecular motion and interactions by R_2 and $R_{1\rho}$ Relaxation Dispersion NMR

Erik Walinda[1], Daichi Morimoto[2], and Kenji Sugase[2]

[1] Department of Molecular and Cellular Physiology, Graduate School of Medicine, Kyoto University, Yoshida Konoe-cho, Sakyo-Ku, Kyoto 606-8501, Japan

[2] Department of Molecular Engineering, Graduate School of Engineering, Kyoto University, Kyoto-Daigaku Katsura, Nishikyo-Ku, Kyoto 615-8510, Japan

Author for correspondence: Kenji Sugase, sugase@moleng.kyoto-u.ac.jp

8 figures

4 tables

~ 11100 words

Keywords: NMR Spectroscopy, Protein dynamics, DNA/RNA dynamics, Chemical exchange, Conformational exchange, Biomolecular interactions, Relaxation Dispersion

Abstract

Among the tools of structural biology, NMR spectroscopy is unique in that it not only derives a static three-dimensional structure, but also provides an atomic-level description of the local fluctuations and global dynamics around this static structure. A battery of NMR experiments is now available to probe the motions of proteins and nucleic acids over the whole biologically relevant timescale from picoseconds to hours. Here we focus on one of these methods, relaxation dispersion, which resolves dynamics on the micro- to millisecond timescale. Key biological processes that occur on this timescale include enzymatic catalysis, ligand binding, and local folding. In other words, relaxation-dispersion-resolved dynamics are often closely related to the function of the molecule and therefore highly interesting to the structural biochemist. With an astounding sensitivity of ~0.5%, the method detects low-population excited states that are invisible to any other biophysical method. The kinetics of the exchange between the ground state and excited states are quantified in the form of the underlying exchange rate, while structural information about the invisible excited state is obtained in the form of its chemical shift. Lastly, the population of the excited state can be derived. This diversity in the information that can be obtained makes relaxation dispersion an excellent method to study the detailed mechanisms of conformational transitions and molecular interactions. Here we describe the two branches of relaxation dispersion, R_2 and $R_{1\rho}$, discussing their applicability, similarities, and differences, as well as recent developments in pulse sequence design and data processing.

1. Introduction

Many life scientists may associate NMR spectroscopy with the structure determination of proteins and other biomolecules; however, a survey of the Protein Data Bank shows that the number of newly determined NMR structures has slightly decreased in recent years (Fig. 1a). While X-ray crystallography and electron microscopy continue to show an upward trend, the primary role of NMR in structural biology has increasingly shifted to address issues other than *de novo* structure determination. In this light, the two main applications of biomolecular NMR now seem to be studying the dynamic motion of biomolecules and deciphering the interactions between molecules. Indeed, in the past ~60 years since the first three-dimensional structures of proteins were deduced [1,2], we have learned that most proteins are actually rather dynamic. Describing them by a single structure can be a helpful and instructive simplification; however, to understand the function of proteins at a detailed level, we must also characterize their conformational dynamics. An important example are enzymes, in which highly concerted conformational changes take place along the catalytic trajectory [3]. Unexpectedly, we also recently learned that seemingly stiff and rigid molecules such as DNA undergo surprising dynamic motions [4].

The success of NMR in elucidating the dynamics of proteins, RNA, and DNA at atomic resolution is not due to a single type of experiment. Over the past decades [5–7], numerous NMR experiments have been developed to study biomolecular dynamics on a wide range of timescales (Fig. 1b). For instance, pico- to nanosecond motions can be resolved by measuring R_1 and R_2 relaxation rates and heteronuclear nuclear Overhauser effect values. Examples of biomolecular motions on these timescales include methyl-group rotation and local dynamics such as loop motion [5,8]. Residual dipolar couplings report on submicro- to millisecond dynamics [9]. Much slower dynamics on the timescale of seconds to hours can be studied by

CLEANEX-PM [10,11], hydrogen-exchange [12], and real-time NMR experiments [13,14]. Frequently, these NMR methods can be integrated with data from other biophysical methods including ultraviolet–visible, Raman, infrared, and fluorescence spectroscopy, time-resolved X-ray crystallography, and molecular dynamics simulations to yield a comprehensive picture of the underlying motion [15,16].

Relaxation dispersion resolves motion on the micro- to millisecond timescale. This time window is particularly interesting from a biochemical point of view because many functionally important dynamic processes, such as a ligand binding to a protein, conformational changes during enzymatic catalysis, and interdomain motions, occur on this timescale. In contrast to pico- to nanosecond motions, which are generally rather localized, the dynamics resolved by relaxation dispersion are often highly correlated motions that have primary importance for the function of the biomolecule.

Here, we provide an overview over the field of relaxation dispersion NMR. A series of examples illustrating the use of the method to understand biomolecular function of various kinds is given in Table 1.

2. Relaxation dispersion

2.1. A brief background and purpose of the method

NMR spectroscopy probes the energy levels of individual atomic nuclei. Therefore, information extracted from NMR experiments is generally obtained in a site-specific manner at atomic resolution. In biomolecules such as proteins, nucleic acids, and carbohydrates, the most commonly studied nuclei are ^{1}H, ^{13}C, and ^{15}N. After Fourier transform, the individual signals of an NMR spectrum have characteristic resonance lines that are rich in information on their dynamic behavior. In a relaxation dispersion experiment, we are quantifying an intensity modulation of the resonance lines. Chemical exchange between a highly populated ground state and one or more "invisible" excited states during a spin-lock or repetitive spin-echo building block of the pulse sequence results in a damping of the peak intensities in a manner that varies with the frequency of the applied field. Thus, we can retrace and study the exchange process in a biological macromolecule by quantifying the peak intensities obtained from a relaxation dispersion experiments, thereby revealing conformational states that are not directly observed in a conventional NMR spectrum.

A relaxation dispersion experiment can yield structural, kinetic, and thermodynamic information about the exchange process and the hidden excited states (Fig. 2). For simplicity, the following discussion assumes the presence of a single excited state. Structural information does not mean that the structure of the excited state is directly obtained; instead, what can be derived is the difference in chemical shift between the ground state (A) and an excited state (B), $\Delta\omega_{AB}$. The excited state chemical shift ω_B can then be interpreted, compared with theoretical or calculated chemical shifts, or used as a restraint in a structure calculation routine. Kinetic information is obtained as the exchange rate between the ground

and excited states, k_{ex}, which is the sum of the reaction rates $k_{A\to B}$ and $k_{B\to A}$ in the exchange process:

$$A \underset{k_{B\to A}}{\overset{k_{A\to B}}{\rightleftharpoons}} B \qquad (1)$$

Lastly, the population of the excited state, p_B, relative to that of the ground state, p_A, can be derived. Strikingly, the excited state can be observed with high sensitivity to a detection limit as low as $p_B \approx 0.5\%$.

It is important to note, however, that not all of these parameters are always obtainable. Due to the nature of the equations governing the chemical exchange process [17], the information accessible from a relaxation dispersion experiment critically depends on the exchange rate. In the case of slow exchange on the chemical shift timescale, it is often possible to obtain all parameters: namely, $\Delta\omega_{AB}$, p_A, p_B, and k_{ex} [7]. For a fast exchange process, by contrast, the populations and $\Delta\omega_{AB}$ are often not accessible because these quantities are obtained as a mixed variable $\Phi_{ex} = p_A p_B \Delta\omega_{AB}^2$, which generally cannot be broken down into its individual components [7]. Unfortunately, Φ_{ex} has no direct physical interpretation; for fast-exchange dynamics, therefore, only the site of the exchange process, its exchange rate k_{ex}, and the intrinsic transverse relaxation rate R_2^0 are available for discussion. Intriguingly, it has been recently shown that this critical limitation may be overcome by off-resonance $R_{1\rho}$ relaxation dispersion experiments, although high-quality experimental data, thorough error estimation, and extremely careful analysis of the flat and local minima-rich χ^2 surface are necessary [18].

2.2. Variants of the relaxation dispersion experiment

Over the years, two distinct approaches to relaxation dispersion have been devised and further developed: R_2 relaxation dispersion and $R_{1\rho}$ relaxation dispersion.

2.2.1. R_2 relaxation dispersion

In the R_2 relaxation dispersion experiment, the effective transverse relaxation rate R_2^{eff}, composed of the intrinsic transverse relaxation rate R_2^0 and an additional contribution from exchange, R_{ex}, is obtained from a Carr–Purcell–Meiboom–Gill (CPMG) [19–21] pulse sequence. In the presence of millisecond-scale chemical exchange, R_2^{eff} varies as a function of the delay, τ_{CP}, between two successive refocusing pulses in the CPMG pulse train (note that some groups define this delay as $2\tau_{CP}$). An R_2 relaxation dispersion profile plots R_2^{eff} as a function of the CPMG pulsing frequency ν_{CPMG} or, alternatively, the inverse delay $\frac{1}{\tau_{\text{CP}}}$ (Fig. 2). Both descriptions are equivalent and can be interconverted as $\frac{1}{\tau_{\text{CP}}} = 2\nu_{\text{CPMG}}$. At high pulsing frequencies, the exchanging coherence is efficiently refocused and high intensity (low R_2^{eff}) signals are obtained. At a low pulsing frequency, refocusing is not as efficient and thus low intensity signals (high R_2^{eff}) are seen. If the spin of interest does not exhibit millisecond exchange, the same value of R_2^{eff} will be obtained (within error) for each CPMG frequency, resulting in a flat relaxation dispersion profile.

Importantly, the inverse statement is not valid, that is: a flat profile does not prove the absence of exchange. For example, consider a backbone amide group in a protein. If the ^{15}N chemical shift difference between two exchanging states is zero, the ^{15}N relaxation dispersion experiment will yield a flat profile. The ^{1}H chemical shift difference may not be zero and a ^{1}H relaxation dispersion experiment would yield a profile that is not flat. Concluding from the flat ^{15}N relaxation dispersion profile that there are no dynamics at this amide site would have been incorrect. Thus, it has to be kept in mind that relaxation dispersion experiments are

insensitive to exchange processes, where Δω is zero. Another limitation is the time window that can be resolved by the CPMG experiment. If the exchange is too fast or too slow, the resulting relaxation dispersion profile would seem to be flat or almost flat, even in the presence of exchange (see section 2.2.3.). An overview of published R_2 relaxation dispersion experiments on different nuclei is given in Table 2.

2.2.2. $R_{1\rho}$ relaxation dispersion

In the second approach, the effective rotating frame relaxation rate $R_{1\rho}^{\mathrm{eff}}$, comprising the intrinsic relaxation rate $R_{1\rho}^{0}$ and the exchange contribution R_{ex}, is measured. Numerous $R_{1\rho}$ relaxation dispersion pulse sequences on different nuclei have been published (Table 2). In principle, the experiment consists of the application of a simple spin-lock for a time T, which is on the order of 30–50 ms. In the presence of the spin-lock, a coherence decays at the effective rotating frame relaxation rate $R_{1\rho}^{\mathrm{eff}}$, which is a function of the applied spin-lock power and the spin-lock offset. Thus, either spin-lock power-dependent or offset-dependent profiles can be obtained (Fig. 3). The offset-dependent profile has the convenient aspect that the signed value of $\Delta\omega_{\mathrm{AB}}$ can be simply read from the profile, although more data points are generally required to obtain a high-quality offset-dependent profile.

2.2.3. Similarities and differences in the approaches

If we choose to vary the spin-lock power and apply the spin-lock on resonance (offset $\Omega = 0$), then $R_{1\rho}^{\mathrm{eff}} = R_{2}^{\mathrm{eff}}$. Moreover, at a very high pulsing frequency, ν_{CPMG}, the pulse train can be considered to be approaching a spin-lock, thereby illustrating the fundamental similarity between the CPMG and spin-lock experiments (Fig. 4). In practice, the spin-lock power must

be lower than that of the CPMG refocusing pulses, as indicated by the decreased height of the spin-lock boxes in the lower part of the panel of Fig. 4. The highest possible spin-lock power is instrument-dependent; trying to apply a higher power can result in power loss due to drooping of the amplifier [22].

An important difference between the two methods is the time window of dynamics that can be resolved by each respective method. Although the time ranges are similar and partially overlapping (Fig. 1b), somewhat faster dynamics can be studied by $R_{1\rho}$ relaxation dispersion because higher effective fields can be applied. The requirement for an exchange process to be observable by relaxation dispersion is that its exchange rate, k_{ex}, is comparable to the maximally achievable effective field, ω_e^{max}:

$$\begin{aligned} &R_{1\rho} \text{ relaxation dispersion} && k_{ex} \cong \omega_e^{max} = 2\pi\nu_e^{max} = \max\left(\sqrt{\omega_1^2 + \Omega^2}\right) \\ &R_2 \text{ relaxation dispersion} && k_{ex} \cong \omega_e^{max} = 2\pi\nu_{CPMG}^{max} = \max\left(\frac{\pi}{\tau_{CP}}\right) \end{aligned} \qquad (2)$$

where Ω denotes the spin-lock offset (frequency difference between the resonance of interest and the spin-lock carrier), and ω_1 refers to the amplitude of the applied spin-lock field. The angular frequencies Ω, ω_1 and ω_e have units of rad s^{-1}, whereas the regular frequencies ν_e and ν_{CPMG} have units of Hz. For a ^{15}N nucleus, for example, the applied field strength in R_2 relaxation dispersion experiments, ν_{CPMG}, commonly ranges from 25 to 1000 Hz. By comparison, on-resonance spin-lock fields as high as 6 kHz have been used in $R_{1\rho}$ relaxation dispersion experiments at a similar lower field limit of ≅ 25 Hz [23,24]. Using an offset Ω > 0 further increases the effective field (eq. 2); however, too large an offset maximizes R_1 over R_2, and thus does not report on chemical exchange.

The differences in experimentally achievable ω_e thus dictate the time resolution of the experiment for fast exchange processes, while the slow exchange limit is given by the order of the relaxation time *T*. So far, the CPMG experiment seems to be more popular among protein NMR spectroscopists; however, the spin-lock experiment has recently been shown to be extremely fruitful in providing unexpected insight into the dynamic internal chemistry of nucleic acids (Table 1).

2.2.4. Relationship of relaxation dispersion to CEST and DEST

Chemical exchange on the millisecond timescale can also be studied by chemical exchange saturation transfer (CEST) or dark state exchange saturation transfer (DEST) [25,26] (Fig. 1b). While the pulse train frequency is varied in CPMG-type relaxation dispersion experiments, CEST experiments vary the position of the B_1 field between experiments. When the varied B_1 field is neither on resonance with the major (A) nor the minor (B) state, the peak intensity of A remains unaltered. However, once the swept B_1 frequency becomes on-resonance with the minor state, then saturation of the minor state decreases the peak intensity of the major state due to chemical exchange between A and B. Thus, plotting the relative (without/with saturation) intensity of the major state over the varied B_1 frequency yields a large dip for the major state and an additional dip for the minor state. This sweeping of the B_1 field to unveil the resonance frequency of the minor state in CEST experiments resembles off-resonance $R_{1\rho}$ relaxation dispersion experiments, which yield a peak corresponding to the minor state, when the offset equals the separation of the major and minor peaks, $\Delta\omega_{AB}$ (Fig. 3). An important distinction between CEST and relaxation dispersion is that chemical exchange is studied using longitudinal magnetization in CEST, whereas relaxation dispersion employs transverse magnetization. Due to the slower decay of longitudinal magnetization,

this means that CEST can be used to study relatively slower processes. CEST resolves kinetic processes most efficiently, when the exchange rate k_{ex} is 20 to 400 s^{-1} [26]. The very similar DEST experiment employs larger B_1 fields (~ 500 – 2000 Hz) than CEST (10 – 100 Hz) and discriminates states by differences in linewidth between the states (ΔR_2^0) instead of the difference in chemical shift ($\Delta\omega_{AB}$) [26]. For example, DEST can resolve the exchange between a monomeric protein having a rather small R_2^0 and a protein oligomer having a very large value of R_2^0. An in-depth comparative discussion of relaxation dispersion, CEST, and DEST is found in ref. [26].

2.3. Pulse sequences for relaxation dispersion

2.3.1. R_2 relaxation dispersion

The heart of the R_2 relaxation dispersion experiment is repeated refocusing of transverse magnetization for a defined relaxation time T by application of the CPMG pulse train. For heteronuclei such as ^{15}N and ^{13}C, this transverse magnetization is generally obtained by an INEPT sequence. The CPMG pulse train that is applied to the prepared coherence is a repeated spin-echo sequence $(\tau—180°—2\tau—180°—\tau)_n$, in which n is an integer. The interval 2τ between the two refocusing 180° pulses is termed τ_{CP}, and it is varied between experiments to obtain R_2^{eff} as a function of the CPMG frequency.

During the CPMG pulse train, in-phase and anti-phase coherences continually interconvert. Thus, apart from the exchange term R_{ex}, the measured effective transverse relaxation rate R_2^{eff} contains contributions from the in-phase transverse relaxation rate R_2^{in} and the anti-phase transverse relaxation rate R_2^{anti}. To average the different contributions of in-phase and anti-phase transverse relaxation, a relaxation-compensation element can be introduced into the middle of the CPMG pulse train [20]. This element converts anti-phase (e.g. $-2H_zN_y$) into in-

phase coherence (e.g. N_x). The net relaxation rate during the relaxation time T is given as the average of R_2^{in} and R_2^{anti}. A simplified pulse program focusing on evolution of a ^{15}N transverse magnetization through the relaxation block is presented in Fig. 5. The full pulse program additionally contains the preparation block INEPT to obtain $-2H_zN_y$, and a t_1 evolution period for frequency labeling of ^{15}N before transferring the coherence back to the amide proton for detection (t_2). Resonance offset effects and pulse imperfections can be sources of artifacts in the measured R_2^{eff}. These artifacts can be alleviated by suitable CPMG phase cycling [27]. For further experimental details, the interested reader is referred to the original publications (Table 2).

2.3.2. $R_{1\rho}$ relaxation dispersion

As summarized in Table 2, a couple of distinct $R_{1\rho}$ relaxation dispersion pulse sequences have been reported. Most of these experiments probe all spins at the same time, similar to CPMG-type experiments, by 2D NMR. However, probing all spins at one time has the inherent limitation that comparably strong spin-lock fields have to be used to achieve suitable locking of all spins at the same time. For example, placing the spin-lock carrier frequency at the center of the ^{15}N spectral region accurately locks on-resonance and near-resonance spins in the xy plane; for the far off-resonance spins, however, the effective field exhibits a considerable tilt, θ, towards the z-axis if the spin-lock is weak relative to the offset ($\tan\theta = \frac{\omega_1}{\Omega}$). A large tilt maximizes the contribution of R_1 (rather than R_2) to $R_{1\rho}^{eff}$, which is not desirable, because chemical exchange is imprinted only on R_2, not on R_1.

To resolve this issue, recently an alternative strategy has gained popularity [23]. In this approach only one spin is probed at a time. As a result, very weak spin-locks ($\omega_1 / 2\pi \simeq 25$ Hz) can be used. Now each spin has its own ^{15}N spin-lock carrier center frequency (on-

resonance). Therefore, each spin is kept in the *xy* plane ($\Omega = 0$) or near the *xy* plane ($\Omega > 0$), even if the spin-lock power is low. Thus, this selective experiment extracts the maximal information on chemical exchange (R_{ex}), while using weak spin-lock fields. This is advantageous because use of a weak spin-lock extends the time resolution of the experiment for studies of slow-exchange processes [23,28].

For simplicity, we will describe the pulse program for the special case of ^{15}N (Fig. 6). After dephasing equilibrium nitrogen magnetization, proton equilibrium magnetization is excited and converted to transverse magnetization. Now, matched weak-power cross-polarization (CP) fields are applied on both channels at the ^{1}H and ^{15}N frequencies of a single ^{1}H–^{15}N amide resonance of interest [29]. This selective CP element transfers proton to nitrogen coherence for the target resonance. The selectivity of the CP element depends on the amplitude of the CP fields, ω_{CP}. Weaker fields have higher selectivity. The smallest CP field amplitudes that still ascertain complete coherence transfer from a spin *I* to a scalar-coupled spin *S* are calculated from the scalar J_{IS}-coupling [29]: $\omega_{CP} / 2\pi = \frac{\sqrt{3}}{4} J_{IS}$. For the ^{1}H–^{15}N amide spin pair, this evaluates to $\omega_{CP} / 2\pi \simeq 40$ Hz. Under ideal circumstances, such as narrow resonance lines and good ^{1}H–^{15}N chemical shift dispersion (either completely isolated peaks or peaks that can be isolated by using a simple delay-90°-gradient filter [23,30]), only the ^{15}N magnetization of a single resonance of interest is obtained. The experiment can then be recorded as a series of 1D spectra [23,28]. More generally, in crowded ^{1}H–^{15}N chemical shift regions, the CP selectivity will not be perfect and nearby signals may be partially excited [30,31]. It is then advisable to collect 2D spectra to avoid obfuscation of the target peak volume by peak overlap [31]. Because only a few points in F_1 have to be acquired to resolve residual peak overlap at a narrow F_1 spectral width of ~100 Hz, measurement time is not markedly affected by the transition from a 1D to a 2D experiment.

After CP, the ^{15}N magnetization of the spin of interest is stored on the *z*-axis and a gradient (G_2) is applied to dephase unwanted residual transverse magnetization. An equilibration period, τ_{eq}, of the order of ~5 ms is then applied to allow the populations of the ground and excited states to reach their equilibrium values. Non-equilibrium values can arise, for example, if $\Delta\omega_{AB}$ is comparably large. In such a case, the CP element may have selected A, but the coherence of B would have been dephased, resulting in perturbed relative populations, $p_A = 1$ and $p_B = 0$. After the equilibration element, transverse magnetization is generated and a spin-lock is applied for a time T of 30~50 ms. Between experiments, the spin-lock power or offset is varied to obtain $R_{1\rho}^{\mathrm{eff}}$ as a function of either of these parameters. Subsequent ^{15}N frequency labeling (optional), coherence transfer back to ^{1}H by INEPT (2D version [31]) or CP (1D version [23,30]), and acquisition conclude the experiment.

2.4. Sample, equipment, and workflow

2.4.1. Sample

Although relaxation dispersion data are generally obtained as 2D spectra, many data points have to be acquired to yield a full profile. Thus, the experiments have a pseudo-3D nature. In fact, the pulse program can be conveniently written as a pseudo-3D version with the third dimension being the relaxation dispersion-specific parameter, e.g., ν_{CPMG}. As a result, the sample requirements for relaxation dispersion are similar to those for conventional 3D triple-resonance NMR experiments. The sample should be a high-purity mono-disperse solution with a concentration of ~1 mM. For proteins and RNA, it should be verified that the sample does not undergo degradation at the measurement temperature or for the duration of the experiment. In the ideal case, the sample solution would be stable at room temperature for a couple of weeks. For simple ^{13}C and ^{15}N experiments, the isotopic enrichment should be as

high as possible, although experiments on unlabeled nucleic acids have been reported [28]; the pulse sequences for several other spin probes dictate more sophisticated isotope labeling schemes (Table 2).

2.4.2. Equipment

Similar to all NMR experiments, highly specialized equipment is necessary to obtain relaxation dispersion data:

- Experimental sample (e.g., ^{15}N-isotope-labeled protein)
- NMR spectrometer (e.g., Bruker Avance 500 MHz or higher magnetic field and/or newer console)
- Cryogenic probe (optional)
- NMR acquisition software (e.g., Bruker TopSpin)
- Relaxation dispersion pulse program
- Software suitable for fitting the experimental data to a theoretical model (Table 3)

For R_2 relaxation dispersion data, it is also advisable to collect data at two different static magnetic fields. Most pulse sequences are generally not included in the default pulse program library of the acquisition software and have to be obtained from the developing laboratory. Pulse programs for ^{15}N-based R_2 and $R_{1\rho}$ relaxation dispersion experiments can be found on the homepage of our laboratory (http://www.moleng.kyoto-u.ac.jp/~moleng_01/nmr/index.html; demo data for R_2 and $R_{1\rho}$ relaxation dispersion experiments and automated analysis software [32] for $R_{1\rho}$ relaxation dispersion are also available).

2.4.3. Workflow for acquisition of relaxation dispersion data

2.4.3.1. R_2 relaxation dispersion

After a specific R_2 relaxation dispersion pulse program for the spin probe of interest is selected and set up, and all pulses are correctly calibrated, the relaxation delay T is chosen. To be traceable, the dynamic process in question must lead to a measurable intensity modulation within the time T. A delay of 30–50 ms is generally appropriate: 50 ms may be a good first choice, with subsequent optimization. A rule of thumb is to choose T so that half of the reference intensity I_0 remains after T, i.e. $I(T) \cong \frac{1}{2} I_0$.

Next, the variable parameter τ_{CP} must be defined. Between experiments, τ_{CP} is varied by changing the loop counter that directs the amount of CPMG cycles during execution of the pulse program. For example, one acquires a set of 20 spectra while varying the number of CPMG cycles as 0, 1, 2, 3, …, 50, which correspond to the τ_{CP} values 0, 25, 12.5, 8.3, …, 0.5 ms for T = 50 ms. A fraction of data points must be acquired in duplicate in order to estimate the experimental error. Once all parameters are set, the experiment can be started by acquiring either the series of 2D spectra in separate measurements or all spectra in a single pseudo-3D experiment.

2.4.3.2. $R_{1\rho}$ relaxation dispersion

Non-selective $R_{1\rho}$ relaxation dispersion experiments are set up equivalently to the CPMG experiment; however, recent selective versions (Fig. 6) apply a slightly different workflow. After setup of the pulse program and calibration of the pulse powers, a high-resolution heteronuclear single-quantum coherence experiment is required to obtain accurate ^{1}H and ^{15}N amide chemical shifts. Only a portion of the residues actually exhibit micro- to millisecond chemical exchange, and these dynamic residues are identified by a screening experiment [32]. Separating screening and acquisition in this way serves to save spectrometer time. The

screening procedure amounts to probing each target resonance by a weak ($\omega_1 / 2\pi \simeq 50$ Hz) and a strong ($\omega_1 / 2\pi \simeq 3000$ Hz) spin-lock, and comparing the peak intensities. In the absence of chemical exchange, these intensities should be equal within experimental error; in the presence of chemical exchange, by contrast, a lower intensity is expected in the weak spin-lock experiment. This process can be visualized as collecting and comparing only the first and last data point of the relaxation dispersion curve shown in Fig. 2.

After the dynamic residues have been identified, the full experiment is started by varying spin-lock power ($\omega_1 / 2\pi \simeq 50$ to 3000 Hz) or offset frequency ($\Omega \simeq -1000$ to 1000 Hz). As in the CPMG experiment, the relaxation time T is 30~50 ms and set to 0 for the reference experiment. In particular, the seemingly tedious procedure of collecting all residues by separate measurements is greatly simplified by acquisition as a pseudo-4D experiment (dimensions: ^{1}H chemical shift, ^{15}N chemical shift, spin-lock power/offset, residue). Moreover, processing of the pseudo-4D dataset from raw data to curve fitting has been automated [32].

An important practical difference from the CPMG experiment is that experimentally applied spin-lock amplitudes have to be empirically determined by a separate measurement because they may not equal the values set in the acquisition software [22].

3. Data analysis and interpretation

3.1. Data analysis

After the NMR measurement, the series of free induction decays collected at varying CPMG frequency (R_2 relaxation dispersion), spin-lock power ($R_{1\rho}$ relaxation dispersion), or spin-lock offset ($R_{1\rho}$ relaxation dispersion) are subjected to Fourier transform. Linear prediction is not used. The peak intensities $I(T)$ are then extracted and the value of R_*^{eff}, in which the asterisk refers to either 2 or 1ρ, is calculated as:

$$R_*^{\mathrm{eff}} = -\frac{1}{T}\ln\frac{I(T)}{I_0} \qquad (3)$$

where T is the length of the relaxation time, and I_0 is the signal intensity in a reference spectrum in which T is set to 0. For a typical ν_{CPMG}- or ω_1-dependent profile, 15~20 data points including repeated measurements for error estimation are necessary. Spin-lock offset-dependent profiles require more (~40) data points. The values of R_*^{eff} are plotted as a function of ν_{CPMG}, ω_1, or Ω, and then fitted to a theoretical equation, yielding the final values for k_{ex}, Δω, and R_*^0, and the relative populations. Error analysis based on standard deviation, jackknife, or Monte Carlo methods is crucial because variations in the individual parameters can be significant even for apparently clean datasets.

When interpreting the results, one may want to separate local motion from correlated motion. In this case, multiple spin probes of residues that are in close vicinity in the secondary (e.g. correlated folding) or tertiary (e.g. correlated structural changes) structure can be combined into a single cluster. A global fit can then be performed in which a parameter such as k_{ex} is defined as a global variable that is identical for all members of the cluster. This type of cluster analysis both reduces the total parameter space by introducing the global

variable(s) and helps with interpretation of the results from a structural biology point of view. For example, a researcher might want to know how fast a given α-helix (cluster) folds relative to other parts of the protein, rather than looking at these parameters for all individual residues of the protein.

3.2. From measurement to results

For the processing of R_2 relaxation dispersion experiments, we have previously reported a straightforward workflow using NMRPipe for data processing, NMRView for peak picking, and GLOVE for curve fitting [33]. Recently, CcpNmr analysis [34] has gained tremendous popularity in the NMR community. Because CcpNmr can write NMRView peak list (.xpk) output files, the GLOVE tools [33] pkfit and cpmg2glove can be used to quickly process data to the curve fitting step. Regarding $R_{1\rho}$ relaxation dispersion experiments, we have recently described an automated toolkit that performs all steps from Fourier transform of the raw data to curve fitting of the final relaxation dispersion profile in a single execution [32].

The theoretical model that is chosen to fit a relaxation dispersion profile needs careful consideration. Researchers have proposed various equations (Table 4), some of which use different approximations and assumptions of the underlying exchange process. The most general form is a full matrix description given by the Bloch–McConnell equations [17]. The numerical solution to this is computationally expensive, but a convenient shortcut is to first obtain values from an approximate model and then solve the full matrix form using these values as initial input parameters.

A suitable approximation of R_2 relaxation dispersion of a two-state exchange process (eq. 1) was derived by Carver and Richards [35]. This equation is valid for both fast and slow exchange regimes. The effective transverse relaxation rate R_2^{eff} is

$$R_2^{\text{eff}} = R_2^0 + \frac{1}{2}\left\{k_{\text{ex}} - \frac{1}{\tau_{\text{CP}}}\cosh^{-1}\left[D_+\cosh\left(\eta_+\right) - D_-\cos\left(\eta_-\right)\right]\right\} \qquad (3)$$

where $D_\pm$, $\eta_\pm$, and Ψ are given by:

$$\begin{aligned} D_\pm &= \frac{1}{2}\left[\pm 1 + \frac{\Psi + 2\Delta\omega_{\text{AB}}^2}{\sqrt{\Psi^2 + \zeta^2}}\right] \\ \eta_\pm &= \tau_{\text{CP}}\sqrt{\frac{1}{2}\left(\pm\Psi + \sqrt{\Psi^2 + \zeta^2}\right)} \\ \Psi &= k_{\text{ex}}^2 - \Delta\omega_{\text{AB}}^2 \\ \zeta &= 2\Delta\omega_{\text{AB}}\left(k_{\text{A}\to\text{B}} - k_{\text{B}\to\text{A}}\right) \end{aligned} \qquad (4)$$

The transverse relaxation rates in the absence of exchange are assumed to be equal for both states, thus $R_{2\text{A}}^0 = R_{2\text{B}}^0 = R_2^0$. This approximation is commonly used, because $k_{\text{ex}} \gg \left|R_{2\text{A}}^0 - R_{2\text{B}}^0\right|$. There are however exceptions: consider for example, a bound state with a large value of R_2^0, such as observed for a monomeric amyloid protein ($R_{2\text{A}}^0 \approx 10\ \text{s}^{-1}$) bound to the surface of a protofibril ($R_{2\text{B}}^0 \approx 20000\ \text{s}^{-1}$) [25]. Equations have been developed to tackle the scenario of unequal $R_{2\text{A}}^0$ and $R_{2\text{B}}^0$ [36]. The population of the excited state, p_{B}, the exchange rate, k_{ex} and the chemical shift difference between states A and B, $\Delta\omega_{\text{AB}}$ (in units of rad s^{-1}), can then be obtained from curve fitting. Examples of relaxation dispersion profiles fitted to eq. 3 are given in Fig. 7.

4. Protein–ligand interactions

So far, we have focused on intramolecular chemical exchange such as interconversion between two distinct conformations of a protein. It is important to note that the use of

relaxation dispersion is not confined to studies of intramolecular phenomena. Indeed, the method is well-suited to study protein–ligand interactions. Analogous to eq. 1, the protein–ligand system can be written

$$A+B \underset{k_{off}}{\overset{[B]k_{on}}{\rightleftharpoons}} AB \qquad (5)$$

where A is a protein and B is an arbitrary ligand (a small chemical compound or a macromolecule). The chemical exchange of the interaction between A and B can be quantified by relaxation dispersion. By redefining $k_{ex} = [B]k_{on} + k_{off}$, and assuming A to be the free (unbound) and AB the bound state, eqs. 3–4 can be employed. Here, the concentration of the unbound ligand, [B], is a new unknown variable that must be determined. If, for example, one wants to determine k_{on} to calculate the dissociation constant K_D, it is necessary to determine [B] in order to separate $[B]k_{on}$ into [B] and k_{on}. This can be achieved by conducting relaxation dispersion experiments at different ratios of protein to ligand [37].

Relaxation dispersion can also provide great insight into protein–ligand interactions that do not follow a simple one-step binding mechanism. In the case of an intrinsically disordered protein (IDP), for example, binding to a target molecule may induce structure formation in the IDP; thus, binding and folding can be coupled. In the case of the interaction between the IDP pKID (a domain of the transcription factor CREB) and the KIX domain of CBP/p300, the binding can be described by a three-state exchange model:

$$A+B \underset{k_{off}}{\overset{[B]k_{on}}{\rightleftharpoons}} \underline{AB} \underset{k_{-1}}{\overset{k_1}{\rightleftharpoons}} AB \qquad (6)$$

where the association is described by the first step, and the folding (k_1) and unfolding (k_{-1}) are described by the second step. Thus, the intermediate state $\underline{AB}$ is bound but not yet completely folded into the final conformation AB. This model has been used to fit relaxation dispersion data from four samples with varying concentration ratios of KIX to pKID at two static fields (Fig. 8). The chemical shift differences between the free and intermediate states, $\Delta\omega_{FI}$, and the free and bound states, $\Delta\omega_{FB}$, were defined as global parameters for each residue. The global folding and unfolding rates were defined by clustering based on secondary structure proximity because residues that are in close proximity in the same secondary structure element are expected to fold and unfold cooperatively. From the site-specific k_{on} and k_{off} rates, site-specific K_D values were calculated. Strikingly, the mean of the site-specific K_D values obtained from relaxation dispersion NMR agreed well with the macroscopic K_D measured by isothermal titration calorimetry [38]. Overall, the experiment shows that pKID uses its unfolded form to engage with KIX and, upon binding to KIX, assumes a partially but not completely folded intermediate, $\underline{AB}$. After the formation of $\underline{AB}$, pKID folds into the final conformation (AB). More examples of the application of relaxation dispersion to the study of protein–ligand interactions have been reported (see refs. [39,40]).

5. Future perspective

Over the past decades, NMR has seen tremendous improvements in probe and console design and electronics, sample labeling techniques, pulse sequences, and analysis software. In particular, the molecular weight of a sample has long been an intrinsic limitation of biomolecular NMR. With the advent of sophisticated labeling schemes and TROSY-based experiments, however, this limitation has been largely overcome. Nevertheless, the use of NMR as a method for *de novo* structure determination seems to be declining in recent years (Fig. 1). As the "easy" structures are already solved today, it is likely that the remaining "difficult" structures of tomorrow will be resolved by cryo-EM and X-ray crystallography. In this light, NMR will continue to make a crucial contribution to the field of structural biology in elucidating the dynamic character of proteins and nucleic acids. The importance of this contribution is reflected in the fact that dynamic interconversion of distinct protein conformations in solution is now part of first-year undergraduate education [41,42].

There is no doubt that relaxation dispersion, the method of choice to study functionally important micro- to millisecond timescale motions, will continue to make important contributions to the understanding of biochemical processes in the future. In particular, the possibility of determining the complete structure of an excited state of a protein in solution is highly intriguing. After all, no other method can derive such an "invisible" structure [43–45]. It would be exciting if NMR hardware, pulse schemes, sample preparation techniques, and analysis software could be optimized to the level that such invisible structures could be reported for many more proteins of biological relevance.

Apart from NMR itself, a convenient development is that standard desktop computers are now powerful enough to solve the Bloch–McConnell equations numerically. Thus, given experimental data of suitable quality, non-approximate results can be obtained. Large

molecules still present substantial challenges. On the NMR side, signal overlap can affect both R_2 and $R_{1\rho}$ relaxation dispersion measurements, but selective spectroscopy [29,31], difference spectroscopy [46], and TROSY methods [47,48] are actively being developed to overcome this limitation. On the preparative side, larger proteins are sometimes expressed and folded relatively poorly in recombinant bacteria, and are more prone to undergo degradation after preparation. Future advances in cell-free expression systems [49] that maximize yield and labeling efficiency, and minimize the cost of an NMR sample are highly anticipated.

A potential disadvantage of relaxation dispersion may be its indirectness. That is, we do not directly "see" the excited state. Even if the method detects the presence of an excited state with a measurable population, it is difficult to give a straightforward answer to the question: what *is* the excited state? In other words, the excited state must be assigned. If $\Delta\omega_{AB}$ including its sign can be obtained, the chemical shift of the excited state may provide an important clue to the nature of the state. For instance, a ^{1}H chemical shift of 8.1 ppm would suggest an unfolded state. Thus, expected or calculated (either by quantum chemistry or semi-empirical approaches [50]) chemical shifts can be used for comparison. Combining the chemical shift information with the CS-ROSETTA approach [51] may also present a powerful strategy. Ideally, some reasonable model for the excited state is available. Such a model might be a ligand-bound form of a protein, or a biomolecule in an unfolded or partially unfolded state. Then equilibrium chemical shift differences ($\Delta\delta$) can be compared to the chemical shift differences obtained from relaxation dispersion ($\Delta\omega$) by plotting $\Delta\omega$ against $\Delta\delta$. A good overall correlation would imply that the chosen model of the excited state is reasonable, while possible outlier residues may identify regions in which the character of the excited state may not be fully represented by the chosen model.

If relaxation dispersion data are acquired at multiple temperatures, a full kinetic–thermodynamic analysis becomes possible and the relative energy levels can be estimated [4]. Energy calculations from molecular dynamics simulations can then be used for comparison, in addition to providing a visual picture of the transition between the ground and excited states. Including other theoretical and experimental biophysical methods, such as fluorescence spectroscopy, time-resolved X-ray crystallography, and site-directed mutagenesis, will further illustrate the sketch of chemical exchange derived by relaxation dispersion.

6.

Figures

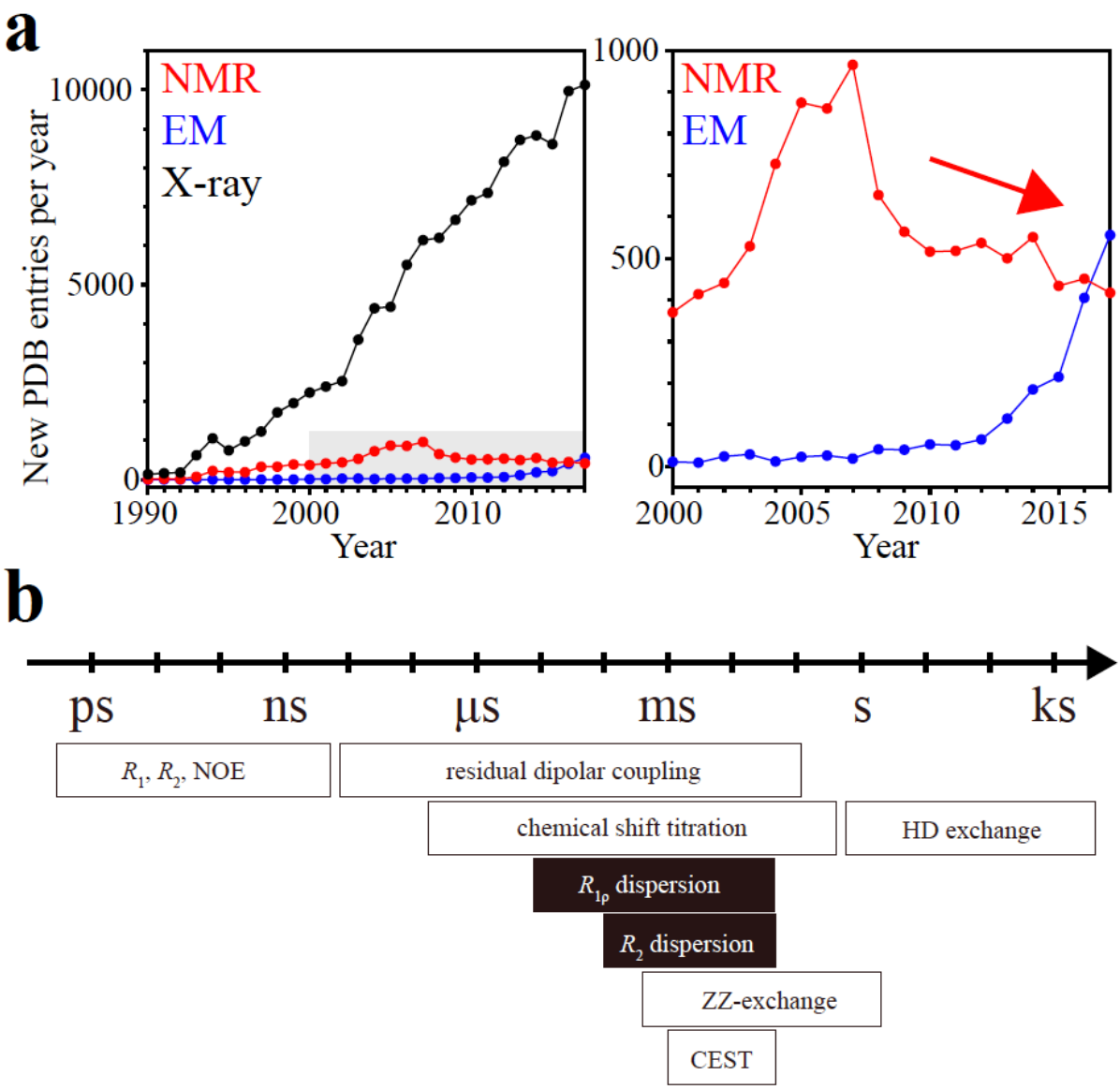

Fig. 1. Resolution of structure and dynamics of biomolecules by NMR. **a.** New structures deposited in the Protein Data Bank by NMR (red), EM (blue), and X-ray crystallography (black). While the number of macromolecular structures determined by X-ray crystallography shows a steady increase (left), since ~2007 the opposite trend is seen for NMR (right, expanded view of the shaded area of the left panel). Source: Protein Data Bank statistics (https://www.rcsb.org/stats/ – Growth of Released Structures Per Year). **b.** NMR experiments

used to detect and quantify molecular motion on various timescales. The two types of relaxation dispersion experiment are highlighted.

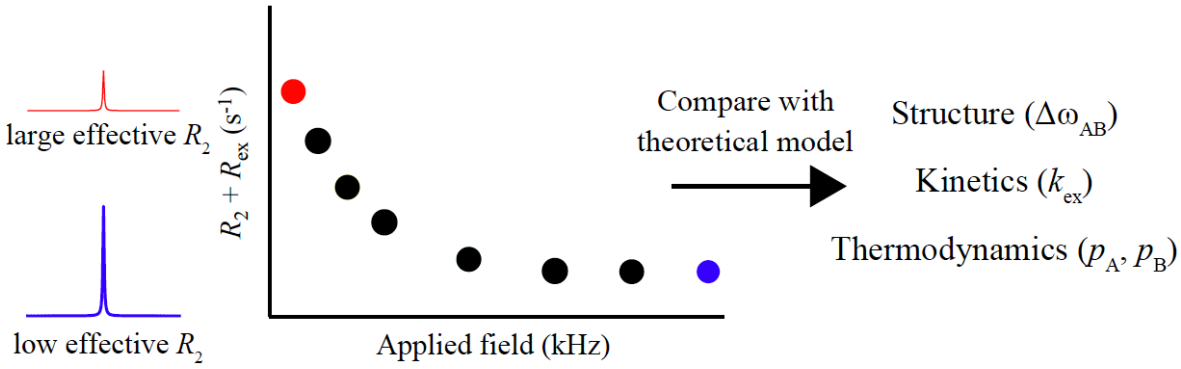

Fig. 2. Relaxation dispersion profile. NMR resonance lines contain information on dynamic exchange processes, for example, the chemical exchange between two distinct conformations A and B in a biomolecule. In a relaxation dispersion experiment, chemical exchange during a fixed delay of the pulse sequence modulates the NMR signal intensities as a function of the amplitude of the applied field. In the presence of chemical exchange, high intensity signals (low effective R_2, blue) are obtained at strong fields, whereas low intensity signals (high effective R_2, red) are observed at weak fields. In the absence of exchange, the signal intensities (and thus R_{ex}) do not vary and a flat profile is obtained. The experimental data points can be fitted to a theoretical model to obtain structural, kinetic, and thermodynamic information on the dynamic process in question.

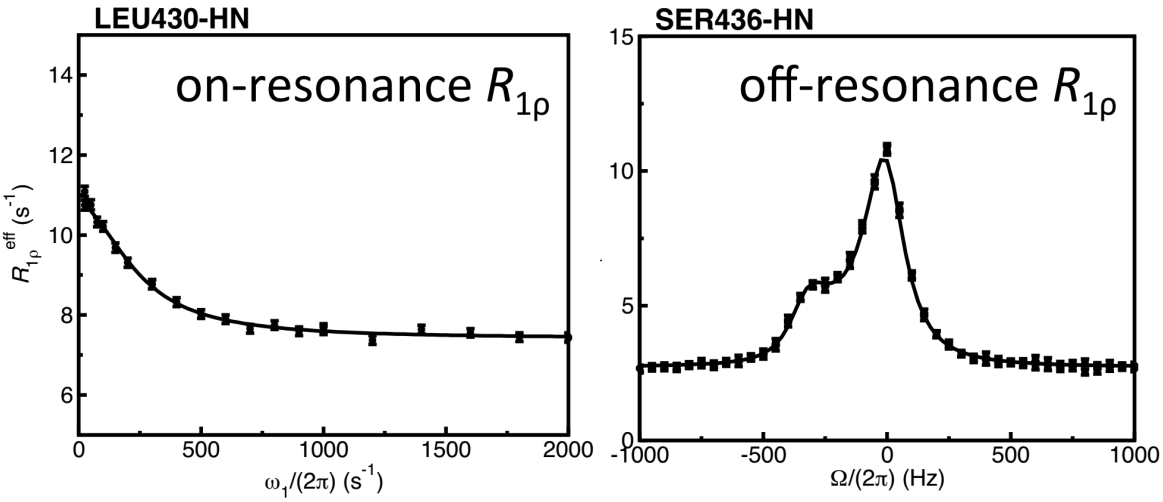

Fig. 3. Examples of $R_{1\rho}$ dispersion profiles. The two variants of the experiment are shown. In the left panel, the spin-lock power is varied; in the right panel, the power is kept constant while the spin-lock offset is varied. Figure reproduced with permission from ref. [32].

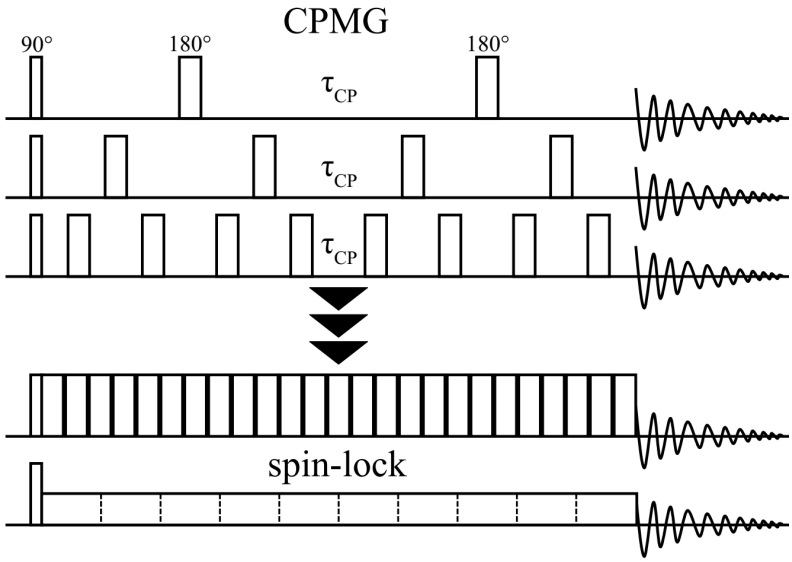

Fig. 4. Visualization of the similarity of CPMG and spin-lock experiments by a thought experiment. The CPMG sequence is shown with decreasing delay, τ_{CP}, between the refocusing pulses. As τ_{CP} is decreased to 0, the CPMG sequence approaches a spin-lock.

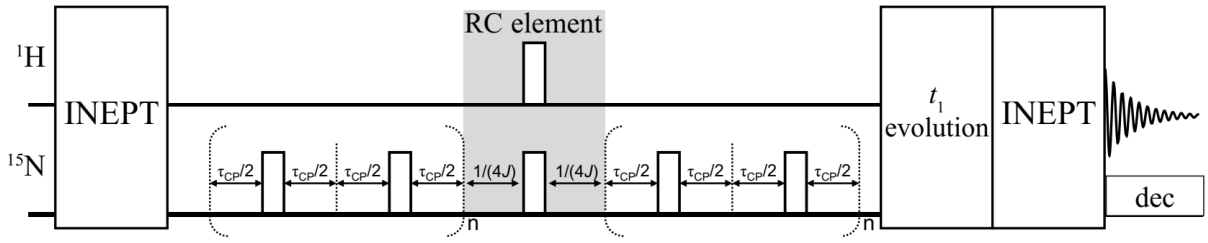

Fig. 5. R_2 relaxation dispersion pulse sequence. A simplified version of the relaxation-compensated ^{15}N CPMG relaxation dispersion experiment [20] is shown with the INEPT, ^{15}N chemical shift evolution, and reverse INEPT steps abbreviated. Open rectangles refer to 180° pulses. dec, decoupling sequence; RC, relaxation compensation.

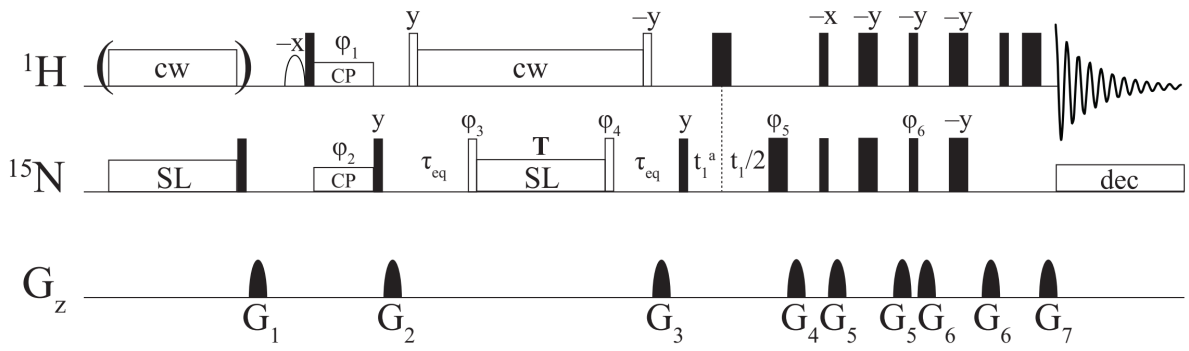

Fig. 6. $R_{1\rho}$ relaxation dispersion pulse sequence. The pulse diagram shows a selective sequence for probing one resonance at a time (reproduced with permission from ref. [31]). Open rectangles denote pulses with varying tip angles [23]; filled rectangles refer to non-selective pulses. CP, cross-polarization; cw, continuous-wave; SL, spin-lock; dec, decoupling sequence. Pulses are applied with either *x*- or the indicated phase.

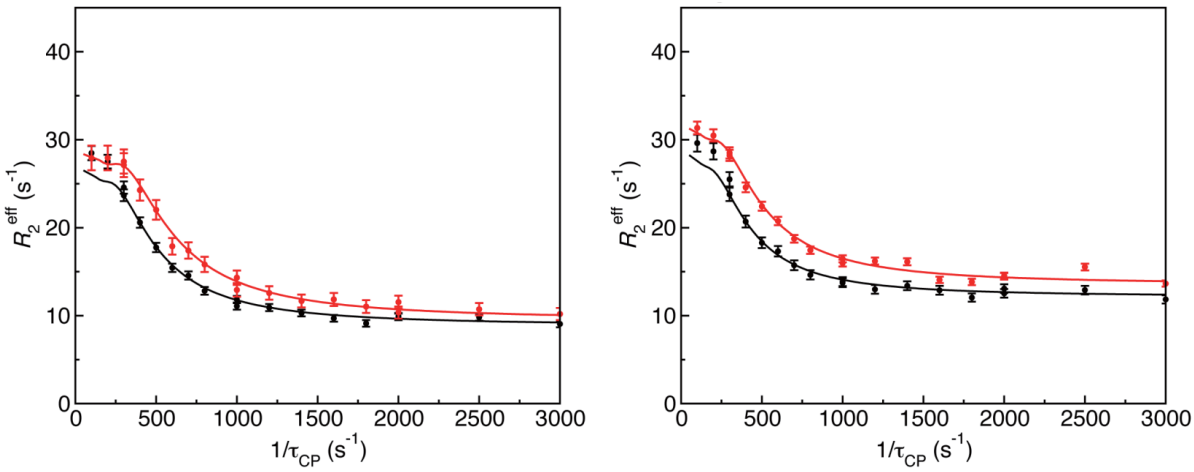

Fig. 7. Examples of R_2 relaxation dispersion data fitted to a theoretical model. The Carver–Richards model was used (solid line). Relaxation dispersion data (filled circles) were collected for the KIX domain of CBP/p300 at two ^{15}N magnetic fields of 60.83 MHz (*black*) and 76.01 MHz (*red*). Figure reproduced with permission from ref. [33].

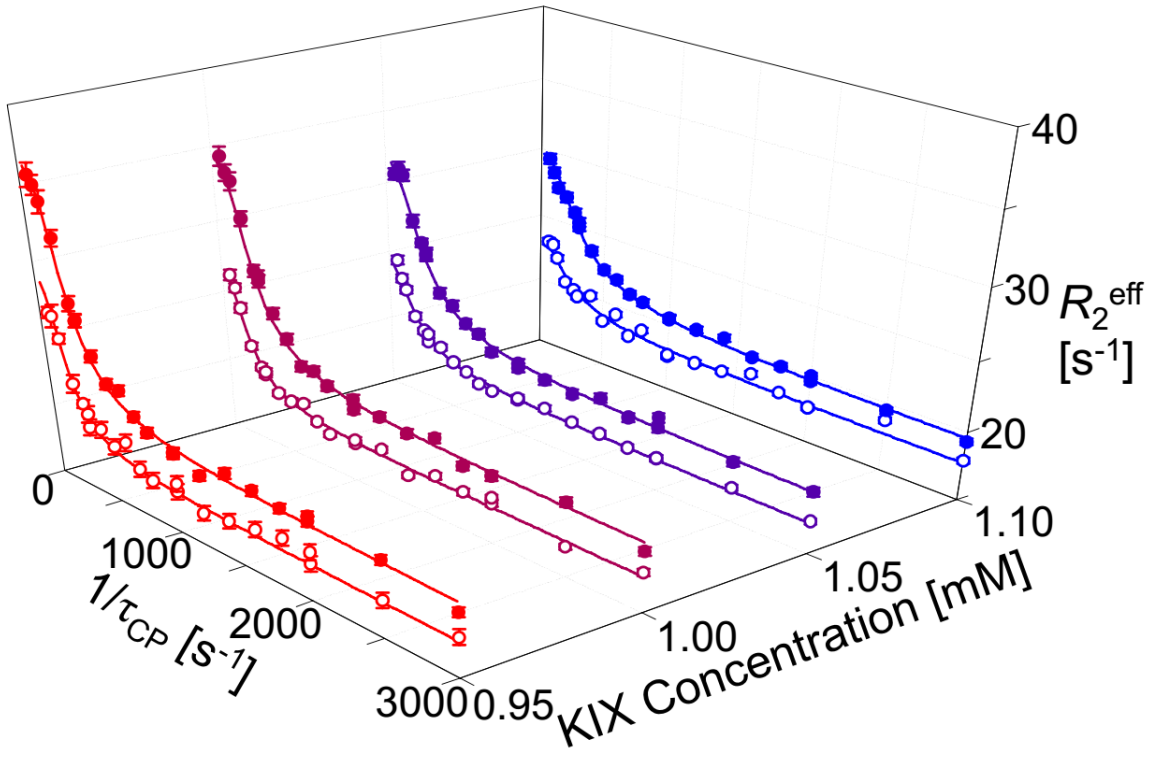

Fig. 8. Using relaxation dispersion to study protein–ligand interactions. R_2 relaxation dispersion profiles (reproduced from [37] with permission) were measured at ^{15}N magnetic fields of 81.08 MHz (filled circles) and 50.65 MHz (open circles). Data for the backbone ^{15}N nucleus of pKID Arg124 are shown. The concentration of pKID was constant (1 mM); the KIX concentration was varied from 0.95 to 1.10 mM. Analysis of the combined dataset yielded k_{on}, k_{off}, k_1, k_{-1}, K_D, $\Delta\omega_{FI}$, and $\Delta\omega_{FB}$.

Tables

Table 1. Examples of biochemical processes studied by relaxation dispersion

Functional process	References
Allosteric regulation	[52,53]
Enzymatic catalysis	[3,54–57]
Folding and binding of intrinsically disordered proteins	[37,40]
Post-translational modification	[58]
Protein folding	[43,59–63]
Structure determination of invisible states	[43–45]
Structural transitions in nucleic acids	[4,64–67]

Table 2. Published relaxation dispersion experiments

	Nucleus	Spin probe	Remarks	Ref.
R_2	^{1}H	Methyl proton		[68,69]
R_2	^{1}H	Amide proton		[70]
R_2	^{1}H	H^{α} proton		[71]
R_2	^{1}H	Side-chain proton		[72]
R_2	^{1}H	Nucleic acid proton		[73]
R_2	^{1}H	Small-molecule ligand proton		[74]
R_2	^{1}H	H^{α} proton	Gly-specific	[75]
R_2	^{13}C	Methyl carbon		[76–79]
R_2	^{13}C	Carbonyl carbon		[80,81]
R_2	^{13}C	Side-chain carbonyl carbon	Asx/Glx-specific	[82]
R_2	^{13}C	Carbonyl carbon		[83,84]
R_2	^{13}C	C_{α} carbon		[85]
R_2	^{13}C	C_{α} carbon	Gly-specific	[75]
R_2	^{13}C	C_{β} carbon		[86]
R_2	^{13}C	Aromatic carbon	TROSY	[87]
R_2	^{15}N	Amide nitrogen		[88]
R_2	^{15}N	Amide nitrogen	^{1}H decoupling	[89]
R_2	^{15}N	Amide nitrogen	Improved ^{1}H decoupling	[90]
R_2	^{15}N	Amide nitrogen	Relaxation compensation	[20,59]
R_2	^{15}N	Amide nitrogen	TROSY	[91]
R_2	^{15}N	Amide nitrogen	Residual dipolar coupling	[92]
R_2	^{15}N	Side-chain nitrogen	Asn/Gln-specific	[93]
R_2	^{31}P	Nucleic acid phosphorus		[94]
R_2	^{13}C-^{1}H	Side-chain methyl ^{13}C-^{1}H	Residual dipolar coupling	[95]
R_2	ZQ, DQ	Amide ^{15}N-^{1}H		[96]
R_2	TQ	Side-chain methyl ^{13}C-^{1}H		[97]
R_2	MQ	Side-chain methyl ^{13}C-^{1}H	TROSY	[47]

R_2	MQ	Amide ^{15}N-^{1}H		[98]
$R_{1\rho}$	^{1}H	Methyl proton		[99]
$R_{1\rho}$	^{1}H	Amide proton		[100–102]
$R_{1\rho}$	^{13}C	Methyl carbon		[103]
$R_{1\rho}$	^{13}C	Carbonyl carbon		[83]
$R_{1\rho}$	^{13}C	C_α carbon		[104]
$R_{1\rho}$	^{13}C	Nucleic acid carbon		[28]
$R_{1\rho}$	^{15}N	Amide nitrogen		[105–107]
$R_{1\rho}$	^{15}N	Amide nitrogen	Adiabatic pulse to align spins	[108]
$R_{1\rho}$	^{15}N	Amide nitrogen	Selective 1D NMR	[23,30]
$R_{1\rho}$	^{15}N	Amide nitrogen	Selective 2D NMR	[31]
$R_{1\rho}$	^{15}N	Amide nitrogen	TROSY	[109]
$R_{1\rho}$	^{15}N	Amide nitrogen	$R_{1\rho} - R_1$	[110]

R_2, CPMG-type R_2 relaxation dispersion experiment; $R_{1\rho}$, spin-lock type $R_{1\rho}$ relaxation dispersion experiment; MQ, multi-quantum coherence; ZQ, zero-quantum coherence; DQ, double-quantum coherence; TQ, triple-quantum coherence.

Table 3. Software packages available for the analysis of relaxation dispersion data

Name	URL	Remarks	Ref.
GLOVE	http://www.scripps.edu/wright/?page_id=17	Open source	[33]
GUARDD	https://code.google.com/archive/p/guardd/	requires MATLAB	[111]
Mathematica	https://www.wolfram.com/mathematica/	Commercial	
MATLAB	https://www.mathworks.com/products/matlab.html	Commercial	
NESSY	https://nmr-nessy.sourceforge.io	Open source	[112]
RELAX	http://www.nmr-relax.com	Open source	[113]

Table 4. Theoretical models to describe relaxation dispersion

	Exchange sites	Remark	Ref.
R_*	N	Complete description (Bloch–McConnell matrix)	[17]
R_2	2	Fast-exchange approximation	[114]
R_2	2	Slow-exchange approximation	[59]
R_2	2	Skewed populations	[115]
R_2	2	All timescales	[35,116]
R_2	2	Exact solution	[117]
R_2	3	Fast-exchange approximation	[118]
$R_{1\rho}$	2	Complete description (Bloch–McConnell matrix)	[17]
$R_{1\rho}$	2	Fast-exchange approximation; On-resonance	[116]
$R_{1\rho}$	2	Fast-exchange approximation; Off-/on-resonance	[119–121]
$R_{1\rho}$	2	Unequal transverse relaxation rates of states A and B	[36]
$R_{1\rho}$	N	Skewed populations; Off-/on-resonance	[122]

Abbreviations

CPMG	Carr–Purcell–Meiboom–Gill
EM	Electron microscopy
NMR	Nuclear magnetic resonance
NOE	Nuclear Overhauser effect
TROSY	Transverse relaxation-optimized spectroscopy

References

[1] M.F. Perutz, M.G. Rossmann, A.F. Cullis, H. Muirhead, G. Will, A.C.T. North, Structure of Haemoglobin: A Three-Dimensional Fourier Synthesis at 5.5Å Resolution Obtained by X-ray Analysis, Nature. 185 (1960) 416–422.

[2] J.C. Kendrew, R.E. Dickerson, B.E. Strandberg, R.G. Hart, D.R. Davies, D.C. Phillips, V.C. Shore, Structure of Myoglobin: A Three-Dimensional Fourier Synthesis at 2Å Resolution, Nature. 185 (1960) 422–427.

[3] D.D. Boehr, D. McElheny, H.J. Dyson, P.E. Wright, The Dynamic Energy Landscape of Dihydrofolate Reductase Catalysis, Science. 313 (2006) 1638–1642.

[4] E.N. Nikolova, E. Kim, A.A. Wise, P.J. O'Brien, I. Andricioaei, H.M. Al-Hashimi, Transient Hoogsteen Base Pairs in Canonical Duplex DNA, Nature. 470 (2011) 498–502.

[5] J. Cavanagh, W.J. Fairbrother, A.J. Palmer, N. Skelton, Protein NMR Spectroscopy: Principles and Practice, Academic Press, New York, 1995.

[6] J.R. Bothe, E.N. Nikolova, C.D. Eichhorn, J. Chugh, A.L. Hansen, H.M. Al-Hashimi, Characterizing RNA Dynamics at Atomic Resolution using Solution-State NMR Spectroscopy, Nat. Methods. 8 (2011) 919–931.

[7] A. Furukawa, T. Konuma, S. Yanaka, K. Sugase, Quantitative Analysis of Protein–Ligand Interactions by NMR, Prog. Nucl. Magn. Reson. Spectrosc. 96 (2016) 47–57.

[8] N. Tjandra, S.E. Feller, R.W. Pastor, A. Bax, Rotational Diffusion Anisotropy of Human Ubiquitin from ^{15}N NMR Relaxation, J. Am. Chem. Soc. 117 (1995) 12562–12566.

[9] O.F. Lange, N.A. Lakomek, C. Fares, G.F. Schröder, K.F.A. Walter, S. Becker, J. Meiler, H. Grubmüller, C. Griesinger, B.L. de Groot, Recognition Dynamics Up to

Microseconds Revealed from an RDC-Derived Ubiquitin Ensemble in Solution, Science. 320 (2008) 1471–1475.

[10] T.L. Hwang, S. Mori, A.J. Shaka, P.C.M. Van Zijl, Application of Phase-Modulated CLEAN Chemical EXchange Spectroscopy (CLEANEX-PM) to Detect Water-Protein Proton Exchange and Intermolecular NOEs, J. Am. Chem. Soc. 119 (1997) 6203–6204.

[11] T.-L. Hwang, P.C.M. van Zijl, S. Mori, Accurate Quantitation of Water-Amide Proton Exchange Rates Using the Phase-Modulated CLEAN Chemical EXchange (CLEANEX-PM) Approach with a Fast-HSQC (FHSQC) Detection Scheme, J. Biomol. NMR. 11 (1998) 221–226.

[12] Y. Bai, J.S. Milne, L. Mayne, W.S. Englander, Primary Structure Effects on Petptide Group Hydrogen Exchange, Proteins. 17 (1993) 75–86.

[13] J. Balbach, V. Forge, N.A.J. van Nuland, S.L. Winder, P.J. Hore, C.M. Dobson, Following Protein Folding in Real Time using NMR Spectroscopy, Nat. Struct. Biol. 2 (1995) 865–870.

[14] A. Furukawa, K. Sugase, R. Morishita, T. Nagata, T. Kodaki, A. Takaori-Kondo, A. Ryo, M. Katahira, Quantitative analysis of location- and sequence-dependent deamination by APOBEC3G using real-time NMR spectroscopy, Angew. Chemie Int. Ed. 126 (2014) 2381–2384.

[15] K.A. Henzler-Wildman, M. Lei, V. Thai, S.J. Kerns, M. Karplus, D. Kern, A Hierarchy of Timescales in Protein Dynamics is Linked to Enzyme Catalysis, Nature. 450 (2007) 913–916.

[16] K.A. Henzler-Wildman, V. Thai, M. Lei, M. Ott, M. Wolf-Watz, T. Fenn, E. Pozharski, M.A. Wilson, G.A. Petsko, M. Karplus, C.G. Hübner, D. Kern, Intrinsic Motions Along an Enzymatic Reaction Trajectory, Nature. 450 (2007) 838–844.

[17] H.M. McConnell, Reaction Rates by Nuclear Magnetic Resonance, J. Chem. Phys. 28

(1958) 430–431.

[18] J.R. Bothe, Z.W. Stein, H.M. Al-Hashimi, Evaluating the Uncertainty in Exchange Parameters Determined from Off-Resonance $R_{1\rho}$ Relaxation Dispersion for Systems in Fast Exchange, J. Magn. Reson. 244 (2014) 18–29.

[19] H.Y. Carr, E.M. Purcell, Effects of Diffusion on Free Precession in Nuclear Magnetic Resonance Experiments, Phys. Rev. 94 (1954) 630–638.

[20] J.P. Loria, M. Rance, A.G. Palmer, A Relaxation-Compensated Carr-Purcell-Meiboom-Gill Sequence for Characterizing Chemical Exchange by NMR Spectroscopy, J. Am. Chem. Soc. 121 (1999) 2331–2332.

[21] S. Meiboom, D. Gill, Modified Spin-Echo Method for Measuring Nuclear Relaxation Times, Rev. Sci. Instrum. 29 (1958) 688–691.

[22] M. Guenneugues, P. Berthault, H. Desvaux, A Method for Determining B_1 Field Inhomogeneity. Are the Biases Assumed in Heteronuclear Relaxation Experiments Usually Underestimated?, J. Magn. Reson. 136 (1999) 118–126.

[23] D.M. Korzhnev, V.Y. Orekhov, L.E. Kay, Off-resonance $R_{1\rho}$ NMR Studies of Exchange Dynamics in Proteins with Low Spin-lock Fields: An Application to a Fyn SH3 Domain, J. Am. Chem. Soc. 127 (2005) 713–721.

[24] D. Ban, A.D. Gossert, K. Giller, S. Becker, C. Griesinger, D. Lee, Exceeding the Limit of Dynamics Studies on Biomolecules Using High Spin-Lock Field Strengths with a Cryogenically Cooled Probehead, J. Magn. Reson. 221 (2012) 1–4.

[25] N.L. Fawzi, J. Ying, R. Ghirlando, D.A. Torchia, G.M. Clore, Atomic-resolution Dynamics on the Surface of Amyloid-β Protofibrils Probed by Solution NMR, Nature. 480 (2011) 268–272.

[26] P. Vallurupalli, A. Sekhar, T. Yuwen, L.E. Kay, Probing Conformational Dynamics in Biomolecules via Chemical Exchange Saturation Transfer: a Primer, J. Biomol. NMR.

67 (2017) 243–271.

[27] G.N.B. Yip, E.R.P. Zuiderweg, A Phase Cycle Scheme that Significantly Suppresses Offset-Dependent Artifacts in the R_2-CPMG ^{15}N Relaxation Experiment, J. Magn. Reson. 171 (2004) 25–36.

[28] A.L. Hansen, E.N. Nikolova, A. Casiano-Negroni, H.M. Al-Hashimi, Extending the Range of Microsecond-to-Millisecond Chemical Exchange Detected in Labeled and Unlabeled Nucleic Acids by Selective Carbon $R_{1\rho}$ NMR Spectroscopy, J. Am. Chem. Soc. 131 (2009) 3818–3819.

[29] P. Pelupessy, E. Chiarparin, Hartmann-Hahn Polarization Transfer in Liquids: An Ideal Tool for Selective Experiments, Concepts Magn. Reson. 12 (2000) 103–124.

[30] E. Walinda, D. Morimoto, M. Shirakawa, K. Sugase, Practical Considerations for Investigation of Protein Conformational Dynamics by ^{15}N $R_{1\rho}$ Relaxation Dispersion, J. Biomol. NMR. 67 (2017) 201–209.

[31] E. Walinda, D. Morimoto, M. Shirakawa, K. Sugase, F_1F_2-Selective NMR Spectroscopy, J. Biomol. NMR. 68 (2017) 41–52.

[32] E. Walinda, D. Morimoto, M. Nishizawa, M. Shirakawa, K. Sugase, Efficient Identification and Analysis of Chemical Exchange in Biomolecules by $R_{1\rho}$ Relaxation Dispersion with Amaterasu, Bioinformatics. 32 (2016) 2539–2541.

[33] K. Sugase, T. Konuma, J.C. Lansing, P.E. Wright, Fast and Accurate Fitting of Relaxation Dispersion Data Using the Flexible Software Package GLOVE, J. Biomol. NMR. 56 (2013) 275–283.

[34] W.F. Vranken, W. Boucher, T.J. Stevens, R.H. Fogh, A. Pajon, M. Llinas, E.L. Ulrich, J.L. Markley, J. Ionides, E.D. Laue, The CCPN Data Model for NMR Spectroscopy: Development of a Software Pipeline, Proteins. 59 (2005) 687–696.

[35] J.P. Carver, R.E. Richards, A General Two-Site Solution for the Chemical Exchange

Produced Dependence of T_2 Upon the Carr-Purcell Pulse Separation, J. Magn. Reson. 6 (1972) 89–105.

[36] A.J. Baldwin, L.E. Kay, An $R_{1\rho}$ Expression for a Spin in Chemical Exchange Between Two Sites with Unequal Transverse Relaxation Rates, J. Biomol. NMR. 55 (2013) 211–218.

[37] K. Sugase, H.J. Dyson, P.E. Wright, Mechanism of Coupled Folding and Binding of an Intrinsically Disordered Protein., Nature. 447 (2007) 1021–1025.

[38] N.K. Goto, T. Zor, M. Martinez-Yamout, H.J. Dyson, P.E. Wright, Cooperativity in Transcription Factor Binding to the Coactivator CREB-Binding Protein (CBP): The Mixed Lineage Leukemia Protein (MLL) Activation Domain Binds to an Allosteric Site on the KIX Domain, J. Biol. Chem. 277 (2002) 43168–43174.

[39] K. Sugase, J.C. Lansing, H.J. Dyson, P.E. Wright, Tailoring Relaxation Dispersion Experiments for Fast-Associating Protein Complexes, J. Am. Chem. Soc. 129 (2007) 13406–13407.

[40] M. Arai, K. Sugase, H.J. Dyson, P.E. Wright, Conformational Propensities of Intrinsically Disordered Proteins Influence the Mechanism of Binding and Folding, Proc. Natl. Acad. Sci. U. S. A. 112 (2015) 9614–9619.

[41] R.L. Tuinstra, F.C. Peterson, S. Kutlesa, E.S. Elgin, M.A. Kron, B.F. Volkman, Interconversion Between Two Unrelated Protein Folds in the Lymphotactin Native State, Proc. Natl. Acad. Sci. U. S. A. 105 (2008) 5057–5062.

[42] J.M. Berg, J.L. Tymoczko, L. Stryer, Biochemistry, 7th ed., W. H. Freeman and Company, New York, 2012.

[43] D.M. Korzhnev, T.L. Religa, W. Banachewicz, A.R. Fersht, L.E. Kay, A Transient and Low-Populated Protein-Folding Intermediate at Atomic Resolution, 329 (2010) 1312–1316.

[44] G. Bouvignies, P. Vallurupalli, D.F. Hansen, B.E. Correia, O. Lange, A. Bah, R.M. Vernon, F.W. Dahlquist, D. Baker, L.E. Kay, Solution Structure of a Minor and Transiently Formed State of a T4 Lysozyme Mutant, Nature. 477 (2011) 111–117.

[45] P. Neudecker, P. Robustelli, A. Cavalli, P. Walsh, P. Lundström, A. Zarrine-Afsar, S. Sharpe, M. Vendruscolo, L.E. Kay, Structure of an Intermediate State in Protein Folding and Aggregation, Science. 336 (2012) 362–366.

[46] T. Konuma, E. Harada, K. Sugase, Extracting Protein Dynamics Information from Overlapped NMR Signals Using Relaxation Dispersion Difference NMR Spectroscopy, J. Biomol. NMR. 63 (2015) 367–373.

[47] D.M. Korzhnev, K. Kloiber, V. Kanelis, V. Tugarinov, L.E. Kay, Probing Slow Dynamics in High Molecular Weight Proteins by Methyl-TROSY NMR Spectroscopy: Application to a 723-Residue Enzyme, J. Am. Chem. Soc. 126 (2004) 3964–3973.

[48] Y. Toyama, M. Osawa, M. Yokogawa, I. Shimada, NMR Method for Characterizing Microsecond-to-Millisecond Chemical Exchanges Utilizing Differential Multiple-Quantum Relaxation in High Molecular Weight Proteins, J. Am. Chem. Soc. 138 (2016) 2302–2311.

[49] E.D. Carlson, R. Gan, C.E. Hodgman, M.C. Jewett, Cell-Free Protein Synthesis: Applications Come of Age, Biotechnol. Adv. 30 (2012) 1185–1194.

[50] S. Neal, A.M. Nip, H. Zhang, D.S. Wishard, Rapid and Accurate Calculation of Protein ^{1}H, ^{13}C and ^{15}N Chemical Shifts, J. Biomol. NMR. 26 (2003) 215–240.

[51] Y. Shen, O. Lange, F. Delaglio, P. Rossi, J.M. Aramini, G. Liu, A. Eletsky, Y. Wu, K.K. Singarapu, A. Lemak, A. Ignatchenko, C.H. Arrowsmith, T. Szyperski, G.T. Montelione, D. Baker, A. Bax, Consistent Blind Protein Structure Generation from NMR Chemical Shift Data, Proc. Natl. Acad. Sci. U. S. A. 105 (2008) 4685–4690.

[52] S.-R. Tzeng, C.G. Kalodimos, Dynamic Activation of an Allosteric Regulatory Protein,

Nature. 462 (2009) 368–372.

[53] S.-R. Tzeng, C.G. Kalodimos, Allosteric Inhibition Through Suppression of Transient Conformational States, Nat. Chem. Biol. 9 (2013) 462–465.

[54] R. Sprangers, A. Gribun, P.M. Hwang, W.A. Houry, L.E. Kay, Quantitative NMR Spectroscopy of Supramolecular Complexes: Dynamic Side Pores in ClpP are Important for Product Release, Proc. Natl. Acad. Sci. U. S. A. 102 (2005) 16678–16683.

[55] K. Henzler-Wildman, D. Kern, Dynamic Personalities of Proteins, Nature. 450 (2007) 964–972.

[56] S.K. Whittier, A.C. Hengge, J.P. Loria, Conformational Motions Regulate Phosphoryl Transfer in Related Protein Tyrosine Phosphatases, Science. 341 (2009) 899–903.

[57] G. Bhabha, J. Lee, D.C. Ekiert, J. Gam, I.A. Wilson, H.J. Dyson, S.J. Benkovic, P.E. Wright, A Dynamic Knockout Reveals That Conformational Fluctuations Influence the Chemical Step of Enzyme Catalysis, Science. 332 (2011) 234–238.

[58] D. Morimoto, E. Walinda, H. Fukada, K. Sugase, M. Shirakawa, Ubiquitylation Directly Induces Fold Destabilization of Proteins, Sci. Rep. 6 (2016) 39453.

[59] M. Tollinger, N.R. Skrynnikov, F.A.A. Mulder, J.D. Forman-Kay, L.E. Kay, Slow Dynamics in Folded and Unfolded States of an SH3 Domain, J. Am. Chem. Soc. 123 (2001) 11341–11352.

[60] P. Neudecker, P. Lundström, L.E. Kay, Relaxation Dispersion NMR Spectroscopy as a Tool for Detailed Studies of Protein Folding, Biophys. J. 96 (2009) 2045–2054.

[61] D.W. Meinhold, P.E. Wright, Measurement of Protein Unfolding/Refolding Kinetics and Structural Characterization of Hidden Intermediates by NMR Relaxation Dispersion, Proc. Natl. Acad. Sci. U. S. A. 108 (2011) 9078–9083.

[62] K. Yanagi, K. Sakurai, Y. Yoshimura, T. Konuma, Y.H. Lee, K. Sugase, T. Ikegami,

H. Naiki, Y. Goto, The Monomer-Seed Interaction Mechanism in the Formation of the β2-Microglobulin Amyloid Fibril Clarified by Solution NMR Techniques, J. Mol. Biol. 422 (2012) 390–402.

[63] D.M. Korzhnev, X. Salvatella, M. Vendruscolo, A.A. Di Nardo, A.R. Davidson, C.M. Dobson, L.E. Kay, Low-populated Folding Intermediates of Fyn-SH3 Characterized by Relaxation Dispersion NMR, Nature. 430 (2004) 586–590.

[64] E.N. Nikolova, F.L. Gottardo, H.M. Al-Hashimi, Probing Transient Hoogsteen Hydrogen Bonds in Canonical Duplex DNA using NMR Relaxation Dispersion and Single-Atom Substitution, J. Am. Chem. Soc. 134 (2012) 3667–3670.

[65] E.A. Dethoff, K. Petzold, J. Chugh, A. Casiano-Negroni, H.M. Al-Hashimi, Visualizing Transient Low-populated Structures of RNA, Nature. 491 (2012) 724–728.

[66] I.J. Kimsey, K. Petzold, B. Sathyamoorthy, Z.W. Stein, H.M. Al-Hashimi, Visualizing Transient Watson-Crick-like Mispairs in DNA and RNA Duplexes, Nature. 519 (2015) 315–320.

[67] I.J. Kimsey, E.S. Szymanski, W.J. Zahurancik, A. Shakya, Y. Xue, C.-C. Chu, B. Sathyamoorthy, Z. Suo, H.M. Al-Hashimi, Dynamic Basis for dG•dT Misincorporation via Tautomerization and Ionization, Nature. 554 (2018) 195–201.

[68] A.J. Baldwin, T.L. Religa, D.F. Hansen, G. Bouvignies, L.E. Kay, $^{13}CHD_2$ Methyl Group Probes of Millisecond Time Scale Exchange in Proteins by ^{1}H Relaxation Dispersion: An Application to Proteasome Gating Residue Dynamics, J. Am. Chem. Soc. 132 (2010) 10992–10995.

[69] R. Otten, J. Villali, D. Kern, F.A.A. Mulder, Probing Microsecond Time Scale Dynamics in Proteins by Methyl ^{1}H Carr-Purcell-Meiboom-Gill Relaxation Dispersion NMR Measurements. Application to Activation of the Signaling Protein $NtrC^{r}$, J. Am. Chem. Soc. 132 (2010) 17004–17014.

[70] R. Ishima, D.A. Torchia, Extending the Range of Amide Proton Relaxation Dispersion Experiments in Proteins using a Constant-Time Relaxation-Compensated CPMG Approach, J. Biomol. NMR. 25 (2003) 243–248.

[71] P. Lundström, D.F. Hansen, P. Vallurupalli, L.E. Kay, Accurate Measurement of Alpha Proton Chemical Shifts of Excited Protein States by Relaxation Dispersion NMR Spectroscopy, J. Am. Chem. Soc. 131 (2009) 1915–1926.

[72] A.L. Hansen, P. Lundström, A. Velyvis, L.E. Kay, Quantifying Millisecond Exchange Dynamics in Proteins by CPMG Relaxation Dispersion NMR Using Side-Chain ^{1}H Probes, J. Am. Chem. Soc. 134 (2012) 3178–3189.

[73] M.A. Juen, C.H. Wunderlich, F. Nußbaumer, M. Tollinger, G. Kontaxis, R. Konrat, D.F. Hansen, C. Kreutz, Excited States of Nucleic Acids Probed by Proton Relaxation Dispersion NMR Spectroscopy, Angew. Chemie Int. Ed. 55 (2016) 12008–12012.

[74] T. Moschen, S. Grutsch, M.A. Juen, C.H. Wunderlich, C. Kreutz, M. Tollinger, Measurement of Ligand–Target Residence Times by ^{1}H Relaxation Dispersion NMR Spectroscopy, J. Med. Chem. 59 (2016) 10788–10793.

[75] P. Vallurupalli, D.F. Hansen, P. Lundström, L.E. Kay, CPMG Relaxation Dispersion NMR Experiments Measuring Glycine $^{1}H^{\alpha}$ and $^{13}C^{\alpha}$ Chemical Shifts in the "Invisible" Excited States of Proteins, J. Biomol. NMR. 45 (2009) 45–55.

[76] N.R. Skrynnikov, F.A.A. Mulder, B. Hon, F.W. Dahlquist, L.E. Kay, Probing Slow Time Scale Dynamics at Methyl-Containing Side Chains in Proteins by Relaxation Dispersion NMR Measurements: Application to Methionine Residues in a Cavity Mutant of T4 Lysozyme, J. Am. Chem. Soc. 123 (2001) 4556–4566.

[77] F.A. Mulder, B. Hon, A. Mittermaier, F.W. Dahlquist, L.E. Kay, Slow Internal Dynamics in Proteins: Application of NMR Relaxation Dispersion Spectroscopy to Methyl Groups in a Cavity Mutant of T4 Lysozyme, J. Am. Chem. Soc. 124 (2002)

1443–1451.

[78] P. Lundström, P. Vallurupalli, T.L. Religa, F.W. Dahlquist, L.E. Kay, A Single-Quantum Methyl ^{13}C-Relaxation Dispersion Experiment with Improved Sensitivity, J. Biomol. NMR. 38 (2007) 79–88.

[79] D.F. Hansen, P. Vallurupalli, L.E. Kay, Measurement of Methyl Group Motional Parameters of Invisible, Excited Protein States by NMR Spectroscopy, J. Am. Chem. Soc. 131 (2009) 12745–12754.

[80] R. Ishima, J. Baber, J.M. Louis, D.A. Torchia, Carbonyl Carbon Transverse Relaxation Dispersion Measurements and ms-μs Timescale Motion in a Protein Hydrogen Bond Network, J. Biomol. NMR. 29 (2004) 187–98.

[81] P. Lundström, D.F. Hansen, L.E. Kay, Measurement of Carbonyl Chemical Shifts of Excited Protein States by Relaxation Dispersion NMR Spectroscopy: Comparison Between Uniformly and Selectively ^{13}C Labeled Samples, J. Biomol. NMR. 42 (2008) 35–47.

[82] A.L. Hansen, L.E. Kay, Quantifying Millisecond Time-Scale Exchange in Proteins by CPMG Relaxation Dispersion NMR Spectroscopy of Side-Chain Carbonyl Groups, J. Biomol. NMR. 50 (2011) 347–355.

[83] F.A.A. Mulder, M. Akke, Carbonyl ^{13}C Transverse Relaxation Measurements to Sample Protein Backbone Dynamics, Magn. Reson. Chem. 41 (2003) 853–865.

[84] P. Vallurupalli, D.F. Hansen, L.E. Kay, Probing Structure in Invisible Protein States with Anisotropic NMR Chemical Shifts, J. Am. Chem. Soc. 130 (2008) 2734–2735.

[85] D.F. Hansen, P. Vallurupalli, P. Lundström, P. Neudecker, L.E. Kay, Probing Chemical Shifts of Invisible States of Proteins with Relaxation Dispersion NMR Spectroscopy: How Well Can We Do?, J. Am. Chem. Soc. 130 (2008) 2667–2675.

[86] P. Lundström, H. Lin, L.E. Kay, Measuring $^{13}C^{\beta}$ Chemical Shifts of Invisible Excited

States in Proteins by Relaxation Dispersion NMR Spectroscopy, J. Biomol. NMR. 44 (2009) 139–155.

[87] U. Weininger, M. Respondek, M. Akke, Conformational Exchange of Aromatic Side Chains Characterized by L-optimized TROSY-Selected ^{13}C CPMG Relaxation Dispersion, J. Biomol. NMR. 54 (2012) 9–14.

[88] V.Y. Orekhov, K. V. Pervushin, D.M. Korzhnev, A.S. Arseniev, Backbone Dynamics of (1-71)Bacterioopsin Studied by Two-dimensional ^{1}H-^{15}N NMR Spectroscopy, Eur. J. Biochem. 219 (1994) 887–896.

[89] D.F. Hansen, P. Vallurupalli, L.E. Kay, An Improved ^{15}N Relaxation Dispersion Experiment for the Measurement of Millisecond Time-Scale Dynamics in Proteins, J. Phys. Chem. B. 112 (2008) 5898–5904.

[90] B. Jiang, B. Yu, X. Zhang, M. Liu, D. Yang, A ^{15}N CPMG Relaxation Dispersion Experiment More Resistant to Resonance Offset and Pulse Imperfection, J. Magn. Reson. 257 (2015) 1–7.

[91] J.P. Loria, M. Rance, A.G. Palmer, A TROSY CPMG Sequence for Characterizing Chemical Exchange in Large Proteins, J. Biomol. NMR. 15 (1999) 151–155.

[92] P. Vallurupalli, D.F. Hansen, E. Stollar, E. Meirovitch, L.E. Kay, Measurement of Bond Vector Orientations in Invisible Excited States of Proteins, Proc. Natl. Acad. Sci. U. S. A. 104 (2007) 18473–18477.

[93] F.A.A. Mulder, N.R. Skrynnikov, B. Hon, F.W. Dahlquist, L.E. Kay, Measurement of Slow (μs-ms) Time Scale Dynamics in Protein Side Chains by ^{15}N Relaxation Dispersion NMR spectroscopy: Application to Asn and Gln Residues in a Cavity Mutant of T4 Lysozyme, J. Am. Chem. Soc. 123 (2001) 967–975.

[94] L.J. Catoire, Phosphorus-31 Transverse Relaxation Rate Measurements by NMR Spectroscopy: Insight Into Conformational Exchange Along the Nucleic Acid

Backbone, J. Biomol. NMR. 28 (2004) 179–184.

[95] A.J. Baldwin, D.F. Hansen, P. Vallurupalli, L.E. Kay, Measurement of Methyl Axis Orientations in Invisible, Excited States of Proteins by Relaxation Dispersion NMR Spectroscopy, J. Am. Chem. Soc. 131 (2009) 11939–11948.

[96] V.Y. Orekhov, D.M. Korzhnev, L.E. Kay, Double- and Zero-Quantum NMR Relaxation Dispersion Experiments Sampling Millisecond Time Scale Dynamics in Proteins, J. Am. Chem. Soc. 126 (2004) 1886–1891.

[97] T. Yuwen, P. Vallurupalli, L.E. Kay, Enhancing the Sensitivity of CPMG Relaxation Dispersion to Conformational Exchange Processes by Multiple-Quantum Spectroscopy, Angew. Chemie Int. Ed. 55 (2016) 11490–11494.

[98] D.M. Korzhnev, K. Kloiber, L.E. Kay, Multiple-Quantum Relaxation Dispersion NMR Spectroscopy Probing Millisecond Time-Scale Dynamics in Proteins : Theory and Application, J. Am. Chem. Soc. 126 (2004) 7320–7329.

[99] U. Weininger, A.T. Blissing, J. Hennig, A. Ahlner, Z. Liu, H.J. Vogel, M. Akke, P. Lundström, Protein Conformational Exchange Measured by ^{1}H $R_{1\rho}$ Relaxation Dispersion of Methyl Groups, J. Biomol. NMR. 57 (2013) 47–55.

[100] R. Ishima, P.T. Wingfield, S.J. Stahl, J.D. Kaufman, D.A. Torchia, Using Amide ^{1}H and ^{15}N Transverse Relaxation to Detect Millisecond Time-Scale Motions in Perdeuterated Proteins: Application to HIV-1 Protease, J. Am. Chem. Soc. 120 (1998) 10534–10542.

[101] P. Lundström, M. Akke, Off-Resonance Rotating-Frame Amide Proton Spin Relaxation Experiments Measuring Microsecond Chemical Exchange in Proteins, J. Biomol. NMR. 32 (2005) 163–173.

[102] C. Eichmüller, N.R. Skrynnikov, A New Amide Proton $R_{1\rho}$ Experiment Permits Accurate Characterization of Microsecond Time-Scale Conformational Exchange, J.

Biomol. NMR. 32 (2005) 281–293.

[103] U. Brath, M. Akke, D. Yang, L.E. Kay, F.A.A. Mulder, Functional Dynamics of Human FKBP12 Revealed by Methyl ^{13}C Rotating Frame Relaxation Dispersion NMR Spectroscopy, J. Am. Chem. Soc. 128 (2006) 5718–5727.

[104] P. Lundström, M. Akke, Microsecond Protein Dynamics Measured by $^{13}C^{\alpha}$ Rotating-Frame Spin Relaxation, ChemBioChem. 6 (2005) 1685–1692.

[105] S. Zinn-Justin, P. Berthault, M. Guenneugues, H. Desvaux, Off-Resonance RF Fields in Heteronuclear NMR: Application to the Study of Slow Motions, J. Biomol. NMR. 10 (1997) 363–372.

[106] D.M. Korzhnev, N.R. Skrynnikov, O. Millet, D.A. Torchia, L.E. Kay, An NMR Experiment for the Accurate Measurement of Heteronuclear Spin-Lock Relaxation Rates, J. Am. Chem. Soc. 124 (2002) 10743–10753.

[107] F. Massi, E. Johnson, C. Wang, M. Rance, A.G. Palmer, NMR $R_{1\rho}$ Rotating-Frame Relaxation with Weak Radio Frequency Fields, J. Am. Chem. Soc. 126 (2004) 2247–2256.

[108] F.A.A. Mulder, R.A. De Graaf, R. Kaptein, R. Boelens, An Off-Resonance Rotating Frame Relaxation Experiment for the Investigation of Macromolecular Dynamics Using Adiabatic Rotations, J. Magn. Reson. 131 (1998) 351–357.

[109] T.I. Igumenova, A.G. Palmer, Off-Resonance TROSY-Selected $R_{1\rho}$ Experiment with Improved Sensitivity for Medium- and High-Molecular-Weight Proteins, J. Am. Chem. Soc. 128 (2006) 8110–8111.

[110] M. Akke, A.G. Palmer, Monitoring Macromolecular Motions on Microsecond to Millisecond Time Scales by $R_{1\rho}$–R_1 Constant Relaxation Time NMR Spectroscopy, J. Am. Chem. Soc. 118 (1996) 911–912.

[111] I.R. Kleckner, M.P. Foster, GUARDD: User-Friendly MATLAB Software for

Rigorous Analysis of CPMG RD NMR Data, J. Biomol. NMR. 52 (2012) 11–22.

[112] M. Bieri, P.R. Gooley, Automated NMR Relaxation Dispersion Data Analysis Using NESSY, BMC Bioinformatics. 12 (2011) 421.

[113] S. Morin, T.E. Linnet, M. Lescanne, P. Schanda, G.S. Thompson, M. Tollinger, K. Teilum, S. Gagné, D. Marion, C. Griesinger, M. Blackledge, E.J. D'Auvergne, Relax: The Analysis of Biomolecular Kinetics and Thermodynamics Using NMR Relaxation Dispersion Data, Bioinformatics. 30 (2014) 2219–2220.

[114] Z. Luz, S. Meiboom, Nuclear Magnetic Resonance Study of the Protolysis of Trimethylamminium Ion in Aqueous Solution - Order of the Reaction with Respect to Solvent, J. Chem. Phys. 39 (1963) 366–370.

[115] R. Ishima, D.A. Torchia, Estimating the Time Scale of Chemical Exchange of Proteins from Measurements of Transverse Relaxation Rates in Solution, J. Biomol. NMR. 14 (1999) 369–372.

[116] D.G. Davis, M.E. Perlman, R.E. London, Direct Measurements of the Dissociation-Rate Constant for Inhibitor-Enzyme Complexes via the $T_{1\rho}$ and T_2 (CPMG) Methods, J. Magn. Reson. Ser. B. 104 (1994) 266–275.

[117] A.J. Baldwin, An Exact Solution for $R_{2,\mathrm{eff}}$ in CPMG Experiments in the Case of Two Site Chemical Exchange, J. Magn. Reson. 244 (2014) 114–124.

[118] M.J. Grey, C. Wang, A.G. Palmer, Disulfide Bond Isomerization in Basic Pancreatic Trypsin Inhibitor: Multisite Chemical Exchange Quantified by CPMG Relaxation Dispersion and Chemical Shift Modeling, J. Am. Chem. Soc. 125 (2003) 14324–14335.

[119] O. Trott, A.G. Palmer, $R_{1\rho}$ Relaxation Outside of the Fast-Exchange Limit, J. Magn. Reson. 154 (2002) 157–160.

[120] O. Trott, D. Abergel, A.G. Palmer, An Average-Magnetization Analysis of $R_{1\rho}$ Relaxation Outside of the Fast Exchange Limit, Mol. Phys. 101 (2003) 753–763.

[121] V.Z. Miloushev, A.G. Palmer, $R_{1\rho}$ Relaxation for Two-Site Chemical Exchange: General Approximations and Some Exact Solutions, J. Magn. Reson. 177 (2005) 221–227.

[122] H. Koss, M. Rance, A.G. Palmer, General Expressions for $R_{1\rho}$ Relaxation for *N*-site Chemical Exchange and the Special Case of Linear Chains, J. Magn. Reson. 274 (2017) 36–45.